Title	Using feedforward digital control to improve the power quality of a three-channel BCM boost converter for PFC applications
Authors	Ryan, Robert T.;Hayes, John G.;Morrison, Richard J.;Hogan, Diarmuid N.
Publication date	2019-03
Original Citation	Ryan, R. T., Hayes, J. G., Morrison, R. J. and Hogan, D. N. (2019) 'Using Feedforward Digital Control to Improve the Power Quality of a Three-Channel BCM Boost Converter for PFC Applications', 2019 IEEE Applied Power Electronics Conference and Exposition (APEC), Anaheim, CA, USA, 17-21 March 2019, pp. 1743-1750. doi: 10.1109/APEC.2019.8722087
Type of publication	Conference item
Link to publisher's version	https://ieeexplore.ieee.org/document/8722087 - 10.1109/APEC.2019.8722087
Rights	© 2019 IEEE. Personal use of this material is permitted. Permission from IEEE must be obtained for all other uses, in any current or future media, including reprinting/republishing this material for advertising or promotional purposes, creating new collective works, for resale or redistribution to servers or lists, or reuse of any copyrighted component of this work in other works.
Download date	2025-09-08 18:38:21
Item downloaded from	https://hdl.handle.net/10468/8319

Using Feedforward Digital Control to Improve the Power Quality of a Three-Channel BCM Boost Converter for PFC Applications

Robert T. Ryan, John G. Hayes
Power Electronics Research Laboratory
School of Engineering
University College Cork
Cork, Ireland
john.hayes@ucc.ie
robertryan@umail.ucc.ie

Richard J. Morrison, Diarmuid N. Hogan
Advanced Energy
27 Eastgate Business Park
Little Island
Cork, Ireland
richard.morrison@aei.com
diarmuid.hogan@aei.com

Abstract—This paper proposes a simple and effective digital feedforward algorithm to improve the power quality of a boundary-conduction-mode (BCM) boost converter for power-factor-correction (PFC) applications. BCM boost converters suffer from a zero-crossing distortion of the line current caused by the valley switching of the converter. The feedforward algorithm works by increasing the switch on-time around the zero crossing of the line voltage, which in turn increases the line current at this point. The feedforward algorithm has a very simple design procedure and implementation requiring only a single look-up table (LUT) in microcontroller software. The algorithm is implemented on a 1 kW interleaved 3-channel BCM boost converter which operates with an input rms line voltage of 85 V to 265 V, and an output voltage of 400 V. Experimental results are given for the prototype converter demonstrating a significantly improved power quality, when the feedforward algorithm is used.

I. INTRODUCTION

For power levels of 300 W and below, the combination of a full-bridge rectifier and BCM boost converter is a popular topology [1]–[3]. Operating the boost converter in BCM creates advantages such as soft-switching, small magnetic volume and a simple control structure that only requires a slow single voltage compensator to regulate the output voltage [4]. At higher power levels the single-channel BCM boost converter suffers from high rms currents which increase conduction losses, and also a high level of differential-mode (DM) electromagnetic-interference (EMI) [5], [6], thus requiring a large DM EMI input filter. A common technique used to extend the power level of the BCM boost converter is to interleave two or three boost converter channels together [7], [8].

The BCM boost converter suffers from a zero-crossing distortion of the line current. This distortion is predominately caused by the valley-switching operation of the converter. Valley switching is when the boost-converter MOS-FET turns on after the energy stored in the MOSFET drain-source capacitor has discharged as much as possible back into the input capacitor of the boost converter. The valley switching results in a slightly negative inductor current at the instant before switch turn on, which distorts the line current causing it to become near zero at the zero crossings of the line voltage. This reduces the converters power quality.

A. Previous Solutions

The most popular solution is to increase the on-time around the zero-crossings using feedforwad control based on the sensed input voltage. Increasing the on-time at the zero-crossing of the line current allows the converter to pull a larger input current at this point, therefore cancelling the effects of the line-current distortion attributed to the valley switching. An analog solution is proposed in [9], where the slope of the pwm-ramp signal is varied with input voltage to increase the on-time at the zero-crossing points. Although this allows for a simple and cost-effective implementation the method must be tuned experimentally for best results. This leads to a difficult design procedure for optimal results. Similarly, in [10] an additional on-time is calculated based on the instantaneous input voltage but must also be tuned experimentally. Another method is to theoretically derive the additional on-time required to cancel the valley switching effects as a function of input voltage only. This is implemented in [11] showing significant improvement in power quality, but requires a complex numerical calculation to calculate the additional on-time needed. Other solutions use more than just the input voltage to estimate the additional on-time required, as in [12] where the optimal additional on-time is calculated as a function of input voltage, switching period and voltage-compensator output. The function is then implemented in microcontroller software but is complex, therefore requiring a high-cost microcontroller. The theoretical waveforms of the inductor current when valley switching occurs are derived in [13]. Based on this analysis the level of distortion in the line current is predicted, and from this an iterative algorithm is used to calculate the additional on-time needed to remove the valley-switching distortion. However, this implementation requires pre-loading different look-up

tables into a microcontroller, and selecting the required on-time as a function of input voltage and input current, resulting in an expensive implementation. Therefore, in [14] the same analysis to derive the optimal on-time is performed, but curve fitting is used to find a simple function based on input voltage only to calculate the additional on-time, allowing for a cheap and simple analog implementation, but also resulting in a complicated design procedure.

B. Proposed Solution

In this paper, a digital feedforward control algorithm is proposed to improve the line current distortion of a 3-channel BCM boost converter. The method is derived based on a theoretical analysis of the valley-switching operation. A feedforward algorithm is derived to calculate the additional on-time required to cancel the valley-switching distortion using only the sensed input voltage. This method allows for a very simple design procedure, does not require any experimental tuning and also has a very cheap implementation as only a single look-up table is needed. The proposed feedforward algorithm provides a good improvement in power quality under all operating conditions.

This paper is structured as follows, Section II gives a brief introduction to the basic operation of the three-channel BCM boost converter and how it is controlled. Section III gives a detailed analysis of the valley-switching operation of the converter. Section IV introduces the simple feedforward algorithm used to reduce the zero-crossing line-current distortion, which is derived from the analysis given in Section III. Finally, in section V experimental results are demonstrated on a 1 kW interleaved 3-channel BCM boost converter to show a significant improvement in the power quality of the converter when the feedforward algorithm is enabled.

II. THREE-CHANNEL BCM BOOST CONVERTER

The power stage circuit diagram of the 3-channel BCM boost converter is depicted in Fig. 1. It consists of a full-bridge rectifier, a small input capacitor C_{in}, three interleaved boost converter channels and a large electrolytic output capacitor C_o. Each boost converter channel has a switch denoted Q_1, Q_2 and Q_3, which are low-cost silicon (Si) MOSFETs, a diode denoted D_1, D_2 and D_3, which are low-cost ultra-fast Si diodes, and a ferrite inductor. Each inductor has an auxiliary winding that is connected to a zero-current detection (ZCD) circuit and is used to trigger the turn-on instant of the switch. The switch turns off after a certain on-time has elapsed.

Fig. 2 demonstrates the typical waveshapes of the input current i_{in} and the inductor currents of each channel i_{L1}, i_{L2} and i_{L3} over a full-line cycle of the line voltage v_{line}. If effects of the valley switching are assumed to be negligible, the average inductor current of each channel can be calculated as

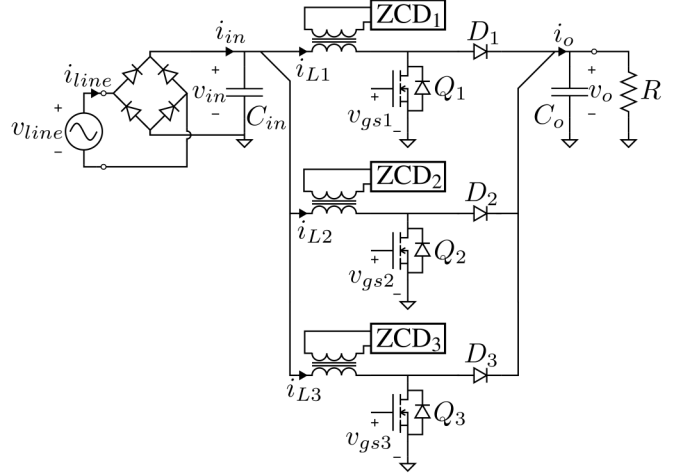$$i_{L(avg)} = \frac{1}{2}i_{L(pk)} = \frac{1}{2}\frac{v_{in}}{L}t_{on} \qquad (1)$$

Fig. 1. Three-channel boost converter power stage.

where $i_{L(pk)}$ is the peak inductor current, v_{in} is the rectified input voltage, L is the boost inductance value and t_{on} is the boost switch on-time.
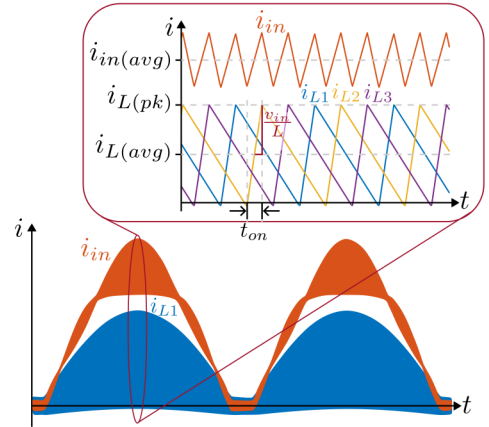

Fig. 2. Typical waveforms of the input current i_{in} and the inductor currents i_{L1}, i_{L2} and i_{L3} over a full-line cycle of the line voltage v_{line}.

The average input current $i_{in(avg)}$ is the sum of the average inductor currents of all channels

$$i_{in(avg)} = \frac{3}{2}\frac{v_{in}}{L}t_{on} \qquad (2)$$

If the on-time remains near constant over a full-line cycle, the average input voltage equals a constant times the rectified input voltage. Therefore $i_{in(avg)}$ and v_{in} have the same shape, and a near-unity power factor is achieved. This is the basis of constant-on-time control [4], which is normally used to regulate the output voltage of BCM boost converters. However, this simplified analysis ignores the effects of the resonance between the MOSFET drain-source capacitance C_{ds} and the boost inductor, which creates a negative inductor current just before MOSFET turn-on. A discussion of how this resonance creates the zero-crossing distortion in the input line current is explained in the next section.

III. Line-Current Distortion

BCM boost converters typically suffer from a line-current zero-crossing distortion. The typical waveshape of the line voltage and line current are shown below in 3. A region exists around the zero-crossing of the line voltage where the line current is zero.
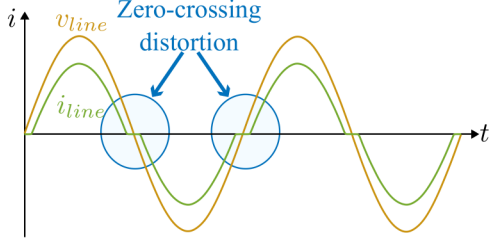

Fig. 3. Typical waveform of the line voltage v_{line} and line current i_{line} for a BCM boost converter with significant zero-crossing distortion.

In order to understand how to reduce the line-current distortion, it is important to understand how it is created. The distortion is predominately caused by the effects of the resonance between the MOSFET drain-source capacitance C_{ds} and the boost inductance L. The resonance has a dramatic effect on the shape of the inductor current waveform.

Fig. 4 shows the circuit diagram of a single channel of the interleaved boost converter, including the MOSFET drain-source capacitance and body diode D_Q.
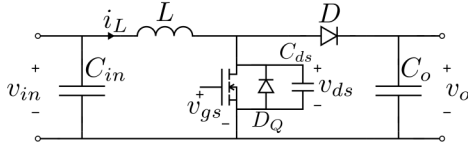

Fig. 4. A single channel of the interleaved boost converter including the MOSFET drain-source capacitance C_{ds} and body diode D_Q.

During a single switching cycle, the boost inductor current charges linearly when the switch is turned. Once a certain on-time has elapsed, the switch turns off and the energy stored in the boost inductor forces the boost diode to be forward biased and charges the output capacitor. When the inductor current has discharged to zero amps, the capacitor C_{ds} is still charged to the output voltage v_o. If the switch remains off, the energy stored in C_{ds} resonates with the boost inductor L. Each boost-converter channel has a zero-current-detection (ZCD) timing circuit that detects when the energy stored in C_{ds} has discharged as much as possible into the boost converter's input capacitor C_{in}. This transfer of energy from C_{ds} to C_{in} during each switching cycle reduces the converter's switching losses. However, this operation also results in the inductor current becoming slightly negative before every MOSFET turn-on instant as is shown in Fig. 5. Fig. 5(a) shows the typical shape of the inductor current over several switching cycles at high instantaneous input voltage, and Fig. 5(b) shows the same waveforms, but at a low instantaneous input voltage.

It can be seen from Fig. 5(b) that the shape of the inductor current has a near-zero average value. As a result, there is a region around the zero-crossing of the line voltage v_{line} where the line current i_{line} is near zero.
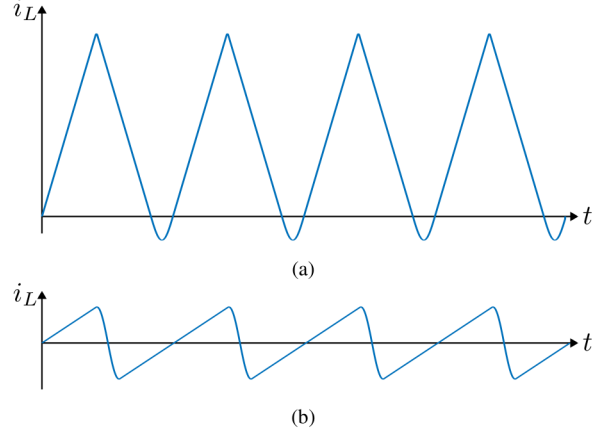

Fig. 5. Inductor current shape at (a) high and (b) low instantaneous input voltages over several switching cycles.

By carrying out a more detailed analysis of the inductor current waveshape over a single switching cycle, it is possible to come up with an additional on-time t_{add}, that must be added to the the on-time t_{on} to cancel the effects of the resonance. There are two possible waveshapes for i_L depending on whether v_{in} is greater than or less than half of the voltage v_o. First we will look at the case when the input voltage is greater then half of the output voltage, this scenario is displayed in Fig. 6.
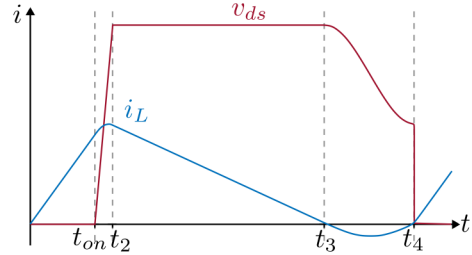

Fig. 6. Waveshape of i_L and v_{ds} over a single switching cycle when $v_{in} > \frac{1}{2}v_o$.

In the time interval $0 \leq t \leq t_{on}$ the MOSFET is switched on, and the inductor is charged linearly by the input voltage. In the interval $t_{on} < t \leq t_2$ the MOSFET is switched off, and the inductor current charges the capacitance C_{ds} until the voltage v_{ds} reaches the same value as v_o and the boost diode D becomes forward biased. In the region $t_2 < t \leq t_3$ the diode D remains forward biased while the energy in the boost inductor discharges into the output capacitor C_o. This continues until $i_L = 0$, and the diode D becomes reversed biased once more. At the instant $t = t_3$, the energy stored in the C_{ds} begins to flow back into the input capacitor C_{in}. This causes the inductor current to become negative in the region $t_3 < t \leq t_4$.

As the capacitance C_{ds} is much smaller than the input capacitance C_{in}, the input voltage can be assumed to be constant over a single switching cycle. Similarly, as the diode's capacitance is much smaller than C_{ds} it is assumed to be negligible. By Kirchoff's voltage law, the following characteristic equation can be written to describe the inductor current and MOSFET drain-source voltage.

$$-v_{in} + L\frac{di_L}{dt} + v_{ds} = 0$$
$$-v_{in} + LC_{ds}\frac{d^2v_{ds}}{dt^2} + v_{ds} = 0 \quad (3)$$

Solving (3), using the initial conditions of $i_L(t_3) = 0$ and $v_{ds}(t_3) = v_o$, and assuming the capacitance C_{ds} is a constant, the following expressions can be written for i_L and v_{ds} as functions of time.

$$i_L(t) = -C_{ds}\omega_r(v_o - v_{in})\sin(\omega_r(t - t_3)) \quad (4)$$
$$v_{ds}(t) = v_{in} + (v_o - v_{in})\cos(\omega_r(t - t_3)) \quad (5)$$

where $\omega_r = \frac{1}{\sqrt{LC_{ds}}}$ is the resonant angular frequency between C_{ds} and L. It is clear from (5) that the voltage v_{ds} reaches a minimum value of $v_{ds} = 2v_{in} - v_o$, this occurs when $t = t_4$. The time instant t_4 occurs at half the resonant period after t_3, so that;

$$t_4 = t_3 + \frac{\pi}{\omega_r} \quad (6)$$

At the instant $t = t_4$ the ZCD circuit triggers the MOSFET to turn back on and the next switching cycle begins. By assuming the additional on-time required to cancel the line-current distortion is equal to the resonant period $t_4 - t_3$, a simple expression is obtained for t_{add} when $v_{in} > \frac{1}{2}v_o$.

In the case where $v_{in} \leq \frac{1}{2}v_o$ the energy stored in C_{ds} can discharge fully until the voltage v_{ds} reaches zero. This condition is shown in Fig. 7. In this case the time instant t_4 is found by setting $v_{ds} = 0$ in (5). Therefore,

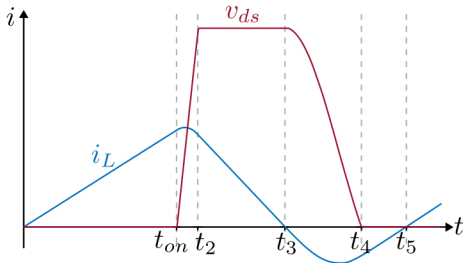$$t_4 = t_3 + \frac{1}{\omega_r}\cos^{-1}\left(\frac{v_{in}}{v_{in} - v_o}\right) \quad (7)$$

Fig. 7. Waveshape of i_L and v_{ds} over a single switching cycle when $v_{in} \leq \frac{1}{2}v_o$.

After $t = t_4$ the negative inductor current forces the MOSFET's body diode D_Q to conduct. This continues until $t = t_5$ when the ZCD circuit triggers the MOSFET turn on, and the next switching cycle begins.

During the interval $t_4 < t \leq t_5$, the inductor current is charged linearly by the input voltage so that $L\frac{di_L}{dt} = v_{in}$, and the inductor current can be described by

$$i_L = \frac{1}{L}\int_{t_4}^{t} v_{in}dt + i_L(t_4)$$
$$= \frac{v_{in}}{L}(t - t_4) + i_L(t_4) \quad (8)$$

When $t = t_5$, the inductor current reaches zero. Therefore, (8) can be used to find an expression for t_5 by setting $i_L(t_5) = 0$.

$$t_5 = t_4 + \frac{Li_L(t_4)}{v_{in}} \quad (9)$$

An expression can be obtained for $i_L(t_4)$ by substituting the value of t_4 obtained in (7) into the expression for i_L obtained in (4).

$$i_L(t = t_4) = -C_{ds}\omega_r(v_o - v_{in})\sin(\omega_r(t_4 - t_3))$$
$$= -C_{ds}\omega_r(v_o - v_{in})\sin\left(\cos^{-1}\left(\frac{v_{in}}{v_{in} - v_o}\right)\right)$$
$$= -C_{ds}\omega_r(v_o - v_{in})\sqrt{1 - \left(\frac{v_{in}}{v_{in} - v_o}\right)^2}$$
$$= C_{ds}\omega_r\sqrt{v_o^2 - 2v_{in}v_o} \quad (10)$$

Combining (9) and (10) the following final expression can be obtained to define the time instant t_5

$$t_5 = t_4 + \frac{1}{\omega_r}\frac{1}{v_{in}}\sqrt{v_o^2 - 2v_{in}v_o} \quad (11)$$

By assuming the additional on-time required to cancel the line-current distortion is equal to the resonant period $t_5 - t_3$, a simple expression is obtained for t_{add} when $v_{in} \leq \frac{1}{2}v_o$.

IV. SIMPLE FEEDFORWARD ALGORITHM

From the earlier analysis in Section III, we can derive the additional on-time t_{add}, which must be added to the on-time calculated by the voltage compensator to cancel the effects of the valley switching. This is done by assuming the additional on-time needed to remove the valley switching distortion is given by $(t_4 - t_3)$ when $v_{in} > \frac{1}{2}v_o$, and $(t_5 - t_3)$ when $v_{in} \leq \frac{1}{2}v_o$. Therefore, the additional on-time can be obtained from (6), (7) and (11) as follows,

$$t_{add} = \frac{\pi}{\omega_r} \qquad \forall \quad v_{in} > \frac{1}{2}V_o$$

$$t_{add} = \frac{1}{\omega_r}\cos^{-1}\left(\frac{v_{in}}{v_{in} - V_o}\right) + ...$$
$$\frac{1}{\omega_r}\frac{1}{v_{in}}\sqrt{V_o^2 - 2v_{in}V_o} \quad \forall \quad v_{in} \leq \frac{1}{2}V_o \quad (12)$$

The term v_o describes the output voltage which varies with time. To simplify the equations, v_o is replaced by the

term V_o in (12). The term V_o is the reference voltage for the voltage compensator and is a constant 400 V. As a result, the feedforward algorithm defined by (12) only has a single variable v_{in}. This allows for a very simple implementation in a digital system as the curve of t_{add} versus v_{in} can be calculated once off, as is done in Fig. 8, over the entire range of v_{in} from 0 to 375 V, and then a single look-up table can be used to calculate t_{add} in the microcontroller software. As the MOSFET used has a non-linear drain-source capacitance that varies with the drain-source voltage, the term ω_r is calculated assuming a contant capacitance given by the time-effective output capacitance from the device datasheet.
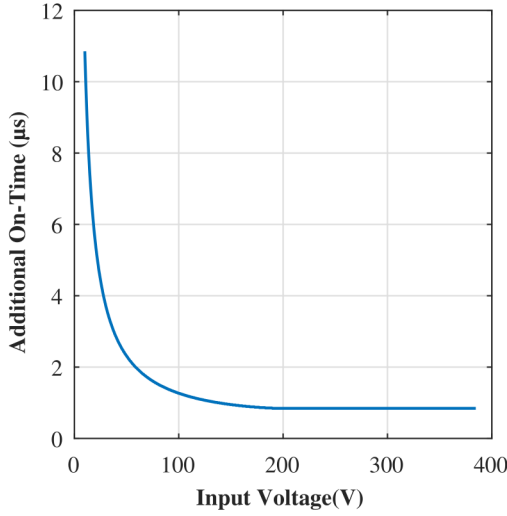

Fig. 8. Additional on-time added by the feedforward algorithm versus input voltage.

Fig. 9 depicts how the feedforward algorithm was implemented as part of the digital control scheme for the 3-channel BCM boost converter. A voltage compensator with a bandwidth of 20 Hz was designed to regulate the output voltage to a constant 400 V. The on-time equals the voltage compensator output v_c plus the additional on-time calculated by the feedforward algorithm per (12), so that $t_{on} = v_c + t_{add}$. The voltage compensator was excuted in an interrupt every 5 kHz. The feedforward algorithm was exected at a rate of 33 kHz. A closed-loop control strategy was implemented to maintain the correct interleaving of the converter [8]. The closed-loop control strategy works by adjusting the individual on-time of each channel t_{on1}, t_{on2} and t_{on3}, to maintain the correct phase-shift.

V. EXPERIMENTAL RESULTS

A 1 kW 3-channel BCM boost converter prototype was built. The main parameters and component values of the prototype converter are given in Table. I. A low-cost XMC1402-Q040X0032 microcontroller from Infineon was used to implement the digital control scheme.

Fig. 10 and Fig. 11 show the output voltage v_o, line voltage v_{line}, input current i_{in} and inductor current of channel
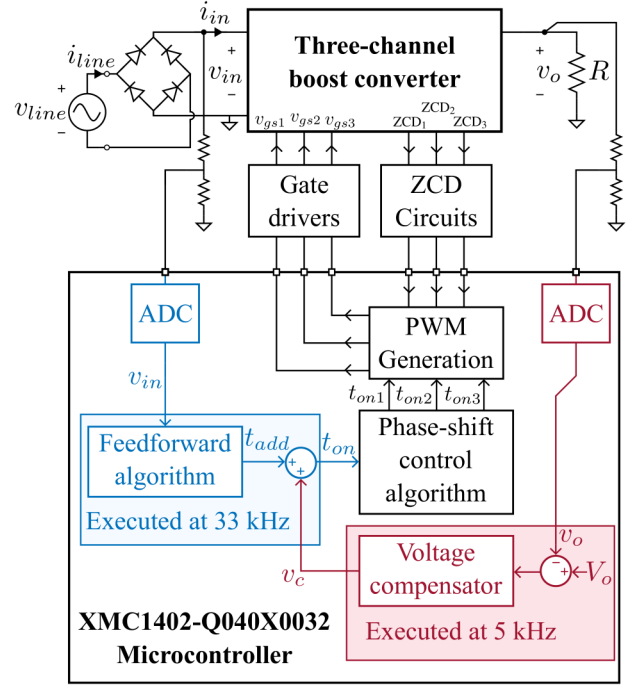

Fig. 9. Three-channel boost converter control circuit.

TABLE I
LIST OF PARAMETERS

Parameter	Value
Microcontroller	XMC1402-Q040X0032
Boost inductance, L	130 μH
Output capacitance, C	880 μF
Input rms voltage	85 V to 265 V
Output voltage, V_o	400 V
Output Power, P_o	0 W to 1000 W
MOSFET	IPA60R099C6
Drain-source capacitance, C_{ds}	550 pF

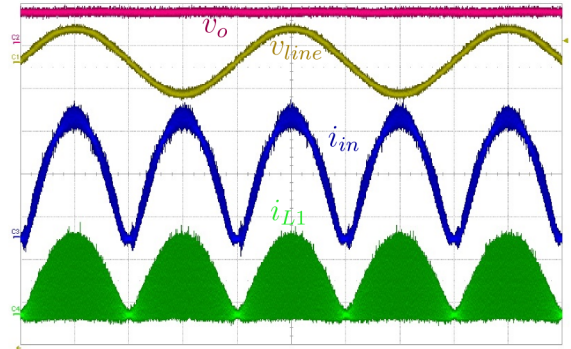one i_{L1}, of the converter under steady-state operation at rms line voltages of 115 V and 230 V, respectively.

Fig. 10. v_o, v_{line}, i_{in} and i_{L1} at $P_o = 800$ W and a 115 V rms line voltage under normal steady-state operation (v_o: 500 V/div, v_{line}: 200 V/div, i_{in}: 2 A/div, i_{L1}: 2 A/div, timebase: 5 ms/div).
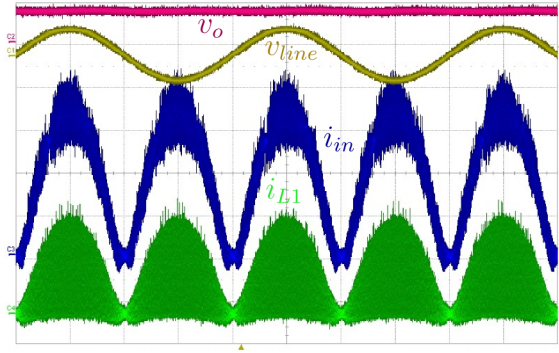
Fig. 11. v_o, v_{line}, i_{in} and i_{L1} at P_o = 1000 W and a 230 V rms line voltage under normal steady-state operation (v_o: 500 V/div, v_{line}: 500 V/div, i_{in}: 2 A/div, i_{L1}: 2 A/div, timebase: 5 ms/div).

To compare the effectiveness of the feedforward control algorithm, the converter was ran with and without the feedforward control algorithm enabled under different conditions. Fig. 12 shows a comparison of the shape of the line voltage and line current i_{line} at 700 W output power and a rms line voltage of 115 V, with and without the feedforward control algorithm implemented. It is clear that when the feedforward algorithm is used the zero-crossing distortion of the line current is significantly reduced.
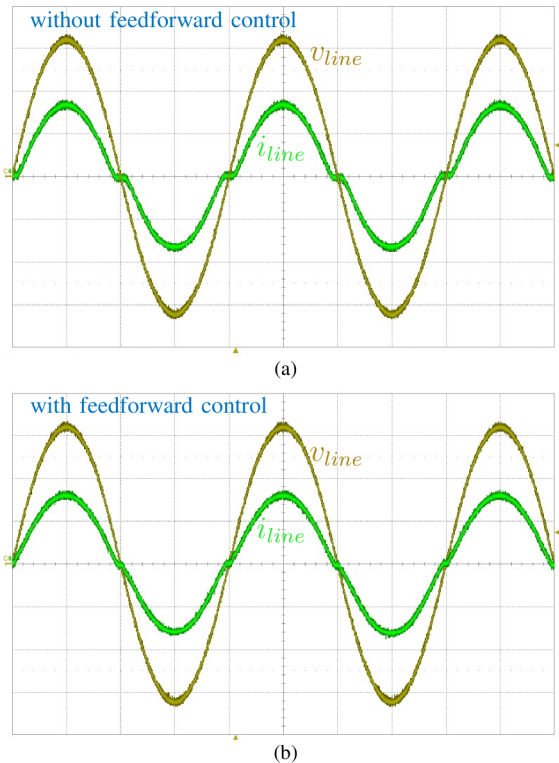

(a)

(b)

Fig. 12. v_{line} and i_{line} at P_o = 700 W and a 115 V rms line voltage (a) without feedforward control and, (b) with feedforward control (v_{line}: 50 V/div, 1_{line}: 5 A/div, timebase: 5 ms/div).

Fig. 13 shows a comparison the line voltage and line

current waveshape with and without the feedforward control enabled for a rms line voltage of 230 V. It is clear from comparing the waveshapes of the line current that there is again significant reduction in the line current zero-crossing distortion when the feedforward control algorithm is implemented.
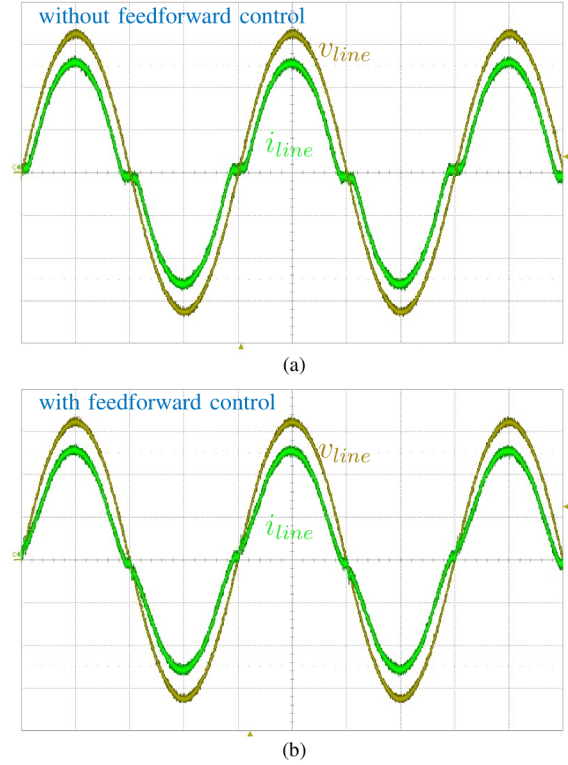

(a)

(b)

Fig. 13. v_{line} and i_{line} at P_o = 900 W and a 230 V rms line voltage (a) without feedforward control and, (b) with feedforward control (v_{line}: 100 V/div, 1_{line}: 2 A/div, timebase: 5 ms/div).

The feedforward control algorithm reduces the line current zero-crossing distortion by drastically increasing the on-time around this point. This increases the average input current drawn by the converter at the line current zero-crossing points. When no feedforward algorithm is used the on-time calculated by the voltage compensator is near constant in steady-state operation. But when the feedforward control algorithm is enabled, there are large variations in on-time as the line voltage changes. This variation of on-time is demonstrated in Fig. 14 and Fig. 15 with and without the feedforward control algorithm enabled at a rms line voltage of 115 V and 230 V respectively.

The power factor of the converter was measured against output power with and without the feedforward control algorithm enabled. This is done in Fig. 16 for a rms line voltage of 115 V, and demonstrats a significant improvement in power factor under all load conditions when the feedforward control is enabled. Similarly, Fig. 17 shows the power factor comparison at 230 V rms line voltage, again with a significant improvement in the converter's power factor under all load conditions.
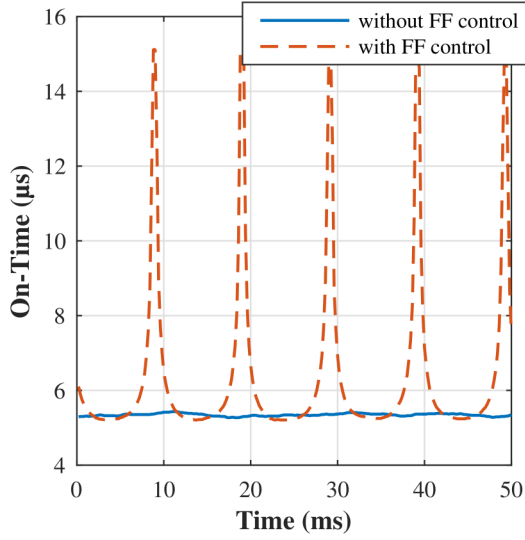
Fig. 14. Measured on-time variation at P_o = 700 W and a rms line voltage of 115 V without feedforward (FF) control (continous line) and with the feedforward (dashed line) control.
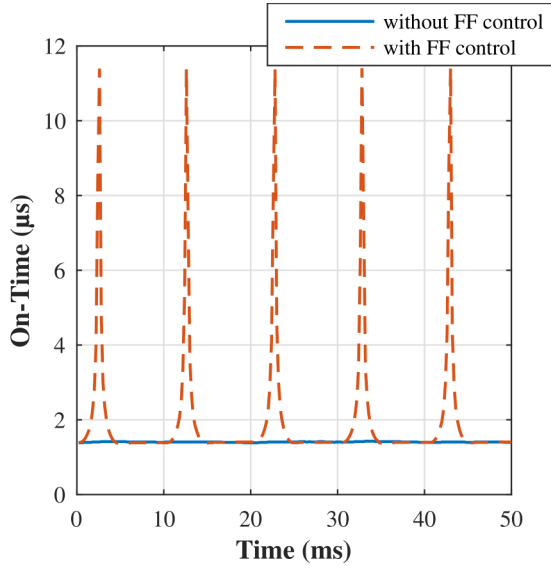

Fig. 16. Power factor comparison without feedforward (FF) control (continuous line) and with feedforward control (dashed line) at 115 V line voltage against output power.

Fig. 15. Measured on-time variation at P_o = 900 W and a rms line voltage of 230 V without feedcforward (FF) control (continous line) and with the feedforward (dashed line) control.

Fig. 17. Power factor comparison without feedforward (FF) control (continuous line) and with feedforward control (dashed line) at 115 V line voltage against output power.

A comparison of the input current harmonics of the converter at rated power and rms line voltag ofe 230 V with and without the feedforward control enabled is given in Fig. 18, demonstrates a substantial reduction in low-order harmonic components. Both sets of input current harmonic measurements are well-below the class A EN61000-3-2 limits.

VI. CONCLUSION

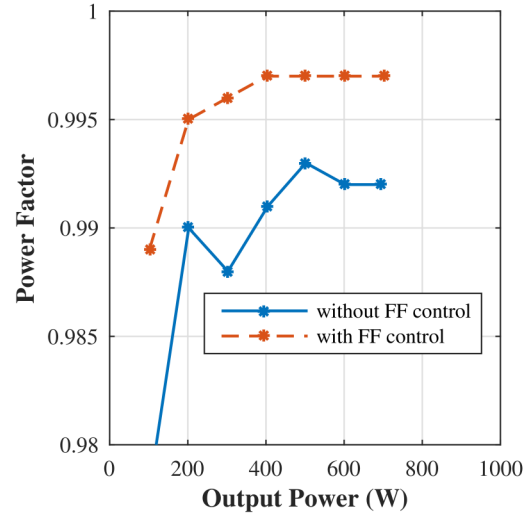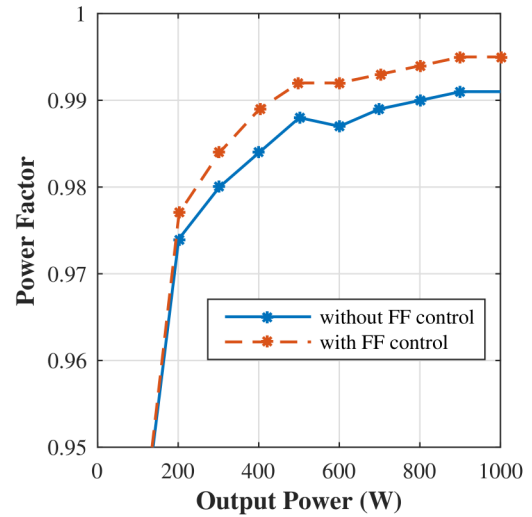A easy-to-implement and effective digital feedforward control algorithm has been presented to improve the power quality of a BCM boost converter for PFC applications. A theoretical analysis of how the valley switching operation creates a zero-crossing distortion of the input line current was performed. This analysis was then used to derive an equation for the additional on-time needed to remove the zero-crossing distortion.

The simple feedforward algorithm was experimentally validated on a 1 kW interleaved 3-channel BCM boost prototype, requiring a very simple implementation where only a single LUT is needed. Experimental results are given comparing the power quality of the converter with and without the feedforward control enabled. The results show the feedforward algorithm provides a significant improvement in power quality under all load and input voltage conditions.
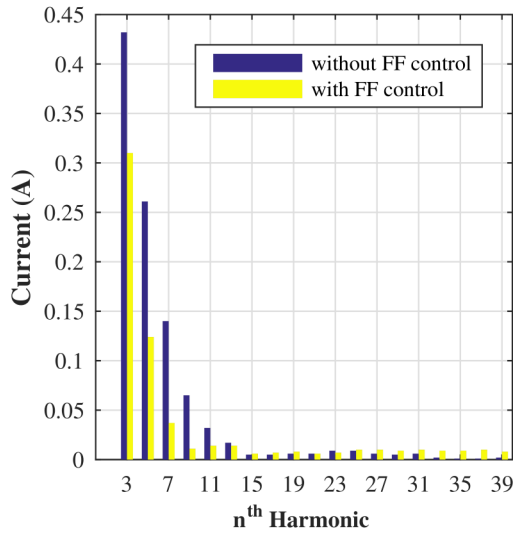
Fig. 18. Power factor comparison without feedforward (FF) control (continuous line) and with feedforward control (dashed line) at $P_o = 1$ kW and a 230 V line voltage against output power.

VII. Acknowledgement

The authors would like to thank Advanced Energy for invaluable support, co-funding and use of equipment during this work. The authors wish to acknowledge the Irish Research Council for co-funding to make this project possible.

References

[1] S. P. Yang, S. J. Chen, and C. M. Huang, "Analysis, modeling and controller design of CRM PFC boost ac/dc converter with constant on-time control IC FAN7530," *IEEE Conference on Industrial Electronics and Applications*, pp. 354–359, Jun. 2014.

[2] N. B. Nam, N. A. Dung, Y.-C. Liu, Y.-C. Hsieh *et al.*, "Design and implementation of digital controlled boost PFC converter under boundary conduction mode," *IEEE International Future Energy Electronics Conference and ECCE Asia*, pp. 1114–1119, Jun. 2017.

[3] J. S. Lai and D. Chen, "Design consideration for power factor correction boost converter operating at the boundary of continuous conduction mode and discontinuous conduction mode," *IEEE Applied Power Electronics Conference and Exposition*, pp. 267–273, Mar. 1993.

[4] R. T. Ryan, J. G. Hayes, R. Morrison, and D. Hogan, "Digital control of an interleaved BCM boost PFC converter with fast transient response at low input voltage," *IEEE Energy Conversion Congress and Exposition*, pp. 257–264, Oct. 2017.

[5] Q. Ji, X. Ruan, and Z. Ye, "The worst conducted EMI spectrum of critical conduction mode boost PFC converter," *IEEE Transactions on Power Electronics*, vol. 30, no. 3, pp. 1230–1241, Mar. 2015.

[6] F. Yang, X. Ruan, Q. Ji, and Z. Ye, "Input differential-mode EMI of CRM boost PFC converter," *IEEE Transactions on Power Electronics*, vol. 28, no. 3, pp. 1177–1188, Mar. 2013.

[7] R. T. Ryan, R. Morrison, D. Hogan, and J. Hayes, "Digital closed-loop control strategy to maintain the phase shift for a multi-channel BCM boost converter for PFC applications," *IEEE Transactions on Power Electronics*, pp. 1–1, 2018.

[8] R. T. Ryan, J. G. Hayes, R. Morrison, and D. Hogan, "A digital closed-loop control strategy for maintaining the 180° phase shift of an interleaved BCM boost converter for PFC applications," *IEEE Energy Conversion Congress and Exposition*, pp. 4927–4934, Oct. 2017.

[9] J. W. Kim, S. M. Choi, and K. T. Kim, "Variable on-time control of the critical conduction mode boost power factor correction converter to improve zero-crossing distortion," *IEEE International Conference on Power Electronics and Drives Systems*, vol. 2, pp. 1542–1546, Nov. 2005.

[10] J. C. Tsai, C. L. Chen, Y. T. Chen, C. L. Ni *et al.*, "Perturbation on-time (POT) technique in power factor correction (PFC) controller for low total harmonic distortion and high power factor," *IEEE Transactions on Power Electronics*, vol. 28, no. 1, pp. 199–212, Jan. 2013.

[11] S. H. Tang, D. Chen, C. S. Huang, C. Y. Liu *et al.*, "A new on-time adjustment scheme for the reduction of input current distortion of critical-mode power factor correction boost converters," *IEEE International Power Electronics Conference and ECCE Asia*, pp. 1717–1724, Jun. 2010.

[12] J. W. Kim, H. S. Youn, and G. W. Moon, "A digitally controlled critical mode boost power factor corrector with optimized additional on time and reduced circulating losses," *IEEE Transactions on Power Electronics*, vol. 30, no. 6, pp. 3447–3456, Jun. 2015.

[13] Z. Guo, X. Ren, H. Gui, Y. Wu *et al.*, "A universal variable on-time compensation to improve THD of high-frequency CRM boost PFC converter," *IEEE Energy Conversion Congress and Exposition*, pp. 1–6, Sep. 2016.

[14] Z. Guo, X. Ren, Y. Wu, Z. Zhang *et al.*, "A novel simplified variable on-time method for CRM boost PFC converter," *IEEE Applied Power Electronics Conference and Exposition*, pp. 1778–1784, Mar. 2017.